# A single-cell atlas reveals tumor heterogeneity and immune environment of acral melanoma

**Jilong Yang** ( yangjilong@tjmuch.com )
Tianjin Medical University Cancer Institute and Hospital https://orcid.org/0000-0001-5162-3740

**Chao Zhang**
Tianjin Medical University Cancer Institute and Hospital

**Hongru Shen**
Tianjin Medical University Cancer Institute and Hospital

**Tielong Yang**
Tianjin Medical University Cancer Hospital & Institute

**Ting Li**
Tianjin Medical University Cancer Hospital & Institute

**Xinyue Liu**
Tianjin Medical University Cancer Hospital & Institute

**Jin Wang**
Tianjin Medical University Cancer Hospital & Institute

**Zhichao Liao**
Tianjin Medical University Cancer Hospital & Institute

**Junqiang Wei**
Tianjin Medical University Cancer Hospital & Institute

**Jia Lu**
Tianjin Medical University Cancer Hospital & Institute

**Haotian Liu**
Tianjin Medical University Cancer Hospital & Institute

**Lijie Xiang**
Tianjin Medical University Cancer Hospital & Institute

**Yichen Yang**
Tianjin Medical University Cancer Institute and Hospital

**Meng Yang**
Tianjin Medical University Cancer Institute and Hospital

**Duan Wang**
Department of Orthopedics Surgery and Orthopedic Research Institute, West China Hospital, Sichuan University, Chengdu

**Yang Li**
Tianjin Medical University Cancer Institute and Hospital https://orcid.org/0000-0001-5142-3853

**Ruwei Xing**
Tianjin Medical University Cancer Institute and Hospital
**Sheng Teng**
Tianjin Medical University Cancer Institute and Hospital
**Jun Zhao**
Tianjin Medical University Cancer Institute and Hospital
**Yun Yang**
Tianjin Medical University Cancer Institute and Hospital
**Gang Zhao**
Department of Pathology, Tianjin Medical University Cancer Institute and Hospital, Tianjin
**Xiangchun Li**
Tianjin Medical University Cancer Institute and Hospital
**Kexin Chen**
Tianjin Medical University Cancer Institute and Hospital

---

**Article**

**Keywords:** Acral melanoma, Single-cell RNA sequencing, Tumor heterogeneity, Immune environment, Cytotoxic CD8+ T cells, Treg cells, PD-1, TIM-3, LAG-3

**Posted Date:** October 25th, 2021

**DOI:** https://doi.org/10.21203/rs.3.rs-690139/v1



---

**Version of Record:** A version of this preprint was published at Nature Communications on November 25th, 2022. See the published version at https://doi.org/10.1038/s41467-022-34877-3.

# Abstract

Acral melanoma is a dismal subtype of melanoma occurring at the extremities of dark-skinned people. We performed single-cell RNA sequencing for 63,394 cells obtained from 5 acral and 3 cutaneous melanoma samples to investigate tumor cellular ecosystem particularly the heterogeneity and immune environment. We defined 5 orthogonal cell clusters that were involved in *TGF-beta* signaling, Type I interferon, Wnt signaling, Cell cycle, and Cholesterol efflux signaling. Signatures of *TGF-beta* signaling and cholesterol efflux are significantly associated with prognosis of melanoma. Compared with cutaneous melanoma, acral melanoma samples had significantly severe immunosuppressive state including depletion of cytotoxic CD8 + T cells, enrichment of Treg cells, and exhausted CD8 + T cells. *PDCD1* (*PD-1*) and *HAVCR2* (*TIM-3*) had higher expression in the exhaustive CD8 + T cells of acral melanoma. In summary, we have uncovered the tumor heterogeneity and immune infiltration characteristics of acral melanoma. Our findings may help to understand and guide the immunotherapy of acral melanoma.


# Introduction

Acral melanoma (AM) is a subtype of melanoma developed in the skin of the extremities such as palm, sole and subungual areas[1,2]. The incidence of acral melanoma is approximately 50% in the Asian population and less than 5% in the European and American populations. Acral melanoma has relatively few single nucleotide mutations without the UV signature, but instead has a genetic landscape characterized by structural rearrangements and amplifications[2]. For instance, acral melanomas have less common *BRAF* and *RAS* mutations and harbor a higher rate of *KIT* mutations and amplification. *KIT* has been considered one of the therapeutic targets in acral melanoma[3]. However, all 6 acral melanoma patients receiving imatinib therapy showed non-response (2 SD and 4 PD) in a phase II studies involving patients with *KIT* mutations[4]. Recent studies showed that anti-PD1 treatment is less effective in acral melanoma[5]. While anti-PD-1 immunotherapy can increase the objective response rate of melanoma to 38%[6], but for acral melanoma it is only 16.6%[7]. Although the somatic copy number profiles and mutational status of selected genes have been detailed in acral melanoma, it is still not clear why acral melanoma does not response well to immunotherapy[3,8]. Therefore, it is needed to further explore the intrinsic features of acral melanoma from other aspects such as the tumor heterogeneity and immune environment by other more accurate methods, such as single-cell sequencing.

The ecological environment of melanoma composes of tumor cells, immune cells, fibroblast cells and endothelial cells etc. Single-cell sequencing provides an unprecedented opportunity to dissecting tumor environment of melanoma. Tirosh and colleagues reported distinct features that had been linked to intrinsic resistance to *RAF/MEK* inhibition[9] in cutaneous melanoma via single-cell sequencing. Andrade and colleagues reported two distinct gene expression programs of natural killer cells that are indicative of significant functional specialization such as cytotoxicity and chemokine synthesis in melanoma[10]. Sade-Feldman and colleagues identified two distinct states of CD8 + T cells that were associated with patient

tumor progression and expression of *TCF7* as a predictor of immunotherapy treatment response in melanoma patients by studying immune cell landscape of melanoma[11]. All these aforementioned studies were dedicated to exploring immune environment and tumor heterogeneity of melanoma. However, single-cell transcriptome profiling of acral melanoma remains unavailable. Therefore, we intended to explore microenvironment of acral melanoma. The purpose of this study is to investigate tumor characteristics and immune environment of acral melanoma and its difference and similarity in comparison with cutaneous melanoma.

# Result

### scRNA-Seq of the ecosystem of acral melanoma by deep learning

We collected 63,394 cells of 5 acral and 3 cutaneous tumor specimens from 6 melanoma patients for scRNA-seq by 10x genomics platform (**Figure 1A**). Detail clinical and pathological information are provided in **Table S1**. The pathological diagnosis of all samples has been reconfirmed by pathologists. There are seven primary and one lymph node metastatic tumor samples. One patient received immunotherapy and the pre- and post-treatment samples were collected (**Figure 1A**).

We identified 50 distinctive cell clusters (**Figure 1B**) that belong to immune cells and non-immune cells. The immune cells were primarily divided into T cells (*CD3D, CD3E*), B cells (*MS4A1, CD79A*), natural killer cells (*FGFBP2, KLRD1*), monocytes and macrophages (*LYZ, CD68, CD14*). The non-immune cell clusters were made up of melanoma cells (*MLANA, PMEL, MITF, DCT*), endothelial cells (*VWF, PECAM1*) and fibroblast cells (*COL1A1, COL3A1*) (**Figure 1D**). We observed that acral melanoma and cutaneous melanoma were distinguishable by the composition of these cell clusters, especially the immune cells (**Figure 1C, 1E**).

### Distinct functional signatures of the melanoma tumor cells

We grouped melanoma tumor cells into 5 main subgroups based on Gene Ontology analysis (See Methods and **Figure 2A, 2B**) and found that these 5 subgroups were characterized by distinct functional signatures (Signature1-5). Signature 1 was involved in cholesterol transportation and phospholipid efflux. Signature 2 was enriched for Wnt signaling pathway and oxidative phosphorylation circuits. Signature 3 was featured by enrichment of Cell cycle circuits such as G2M checkpoint and E2F targets. Signature 4 was associated with *TGF-β signaling*. Signature 5 was enriched for interferon response (**Figure 2C**).

### Pseudo-temporal transition trajectory of melanoma tumor cells

In pseudo-time analysis, we randomly selected 5000 high-quality tumor cells to establish a pseudo-temporal ordering reflective of cell lineage (See Methods). Our result showed that the aforementioned 5 tumor cell subgroups were in different developmental states. Melanoma cells from Subgroups 2 and 3 were mainly at the root of phylogenetic tree. This might indicate that cell from Subgroups 2 and 3 were likely to be primitive tumor cells. Melanoma cells from Subgroups 1, 4 and 5 were at the mid-end of development with better differentiation (**Figure 2D**). We also investigated the transcriptional changes associated with transitional states and observed that melanoma cells could be categorized into 3 pseudo-temporal phases. Phase 1 was predominated by Subgroups 2 and 3, which is characterized by upregulated genes expression of *UQCRH*, *PSMA7*, *LDHA* and *NDUFC2* (**Figure 2E**). Phase 2, predominated by Subgroup 1, was characterized by upregulation of *APOE, APOC1 and PLTP*. Phase 3 was dominated by Subgroups 4 and 5 upregulated by genes associated with Type I interferon signaling (*IFIT3, IFIT2, IRF1*) and heat response (*HSPA1A, HSPA1B*) **(Figure 2E)**.

## Prognostic significance of melanoma cells

For the 6 patients enrolled for scRNA-seq in this study, 3 deceased patients (Cluster1, C1) were featured by overrepresentation of Signatures 2 and 3, while the other 3 patients (Cluster 2, C2) who are alive were enriched for Signatures 1, 4 and 5 (**Figure 2F-2H**). We further examined the association of these signatures with survival in the TCGA SKCM cohort[12]. We divided 452 patients from TCGA skin cutaneous melanoma cohort into G1/2 groups based on enrichment score of the aforementioned five functional signatures (See Methods). The G2 group was enriched for Signatures 1, 4 and 5, while the G1 group was enriched for Signatures 2 and 3 (**Figure 2I**). The G2 group has better overall survival outcome in comparison with G1 group (**Figures 2J;** Log-rank test, HR =0.50, 95% CI: 0.38-0.67, p = 1.47e−06).

In addition, we observed that these five expression signatures of acral melanoma were distinct from cutaneous melanoma (**Figure 2K**). For these 6 patients, 4 patients with acral melanoma patients were enriched for Signatures 1 and 4 while the other 2 cutaneous melanoma patients were enriched for Signature 2 (**Figure 2F**). Therefore, we speculated that patients with acral melanoma may have better survival than those with cutaneous melanoma. This speculation was verified by survival analysis of 602 melanoma patients collected from Tianjin Cancer Hospital (Log-rank test, HR = **1.86**, 95%CI: 1.47-2.34, p = 9.18e-08; **Figure 2L**).

## Immune microenvironment of acral melanoma

We divided the 16011 cells from cell clusters that were annotated to be immune cells **(Figure 1B)** into 50 clusters and subsequently grouped them into 6 cell types (**Figure 3A, see Methods**). The identified cell clusters were featured by distinct marker genes (**Figure 3B**). The T cell cluster consisted of 5 CD4+ T cell subgroups, 8 CD8+ T cell subgroups and Cell cycle T cells (**Figure 3C**). The Treg subgroup highly

expressed *IL2RA, FOXP3* and *IKZF2*, co-stimulatory (*CD28, TNFRSF9* and *ICOS*) and inhibitory markers (*TIGIT, CTLA4 and LAYN*). The CD4-CCR7, CD4-LEF1 and CD8-CCR7 subgroups were naïve T cells, which were marked with expression of *CCR7, LEF1* and *SELL* genes. The CD4-NR4A1 and CD8-NR4A1 subgroup were tissue-resident memory T cells that were featured by high expression of *CD69* and *NR4A1*. The cytotoxic T cell subgroups consisted of CD8-GZMK and CD8-MT1E that were characterized by high expression of *GZMK*, *GZMA*, *GNLY* and *NKG7*, and low expression of genes in involved in immune checkpoint mediation such as *HAVCR2(TIM-3), PDCD1(PD-1)* and *LAG3*. CD8-PDCD1 and CD8-LAG3 subgroups were immunosuppressive CD8+ T cells that were marked with high expression of *CTLA4*, *HAVCR2 (TIM-3), PDCD1 (PD-1)*, *LAG3* and *TIGIT* (**Figure 3C**).

Acral melanoma was featured by higher abundance of the Tregs subgroup and lower abundance of CD4-IL2 subgroups as compared to cutaneous melanoma (**Figure 3D**). None of the other T cell subgroups showed significant differences in acral melanoma versus cutaneous melanoma. In addition, CD8-MT1E, which is a new CD8+ T cell subgroup, was characterized by high expression of *MT1E* and *MT2A* and enriched in two deceased acral melanoma patients.

## CD8+ T cells reside in different transition trajectory states in acral melanoma versus cutaneous melanoma

We applied Monocle[13] to construct the developmental trajectories of the six aforementioned CD8+ T cell subgroups (see **Methods**). The results showed that the pseudo-time trajectory initiates with CD8-CCR7 and CD8-NR4A1 subgroups via an intermediate state (i.e. CD8-GZMK and CD8-MT1E subgroups), and ends in the exhausted state (i.e. CD8-PDCD1 and CD8-LAG3 subgroups) (**Figure 4A**). Starting with the naive signature, the cytotoxic signature continued from the middle of the trajectory towards the end, and the exhausted signature was predominantly upregulated at the end **(Figure 4B**). Meanwhile, we found that the early and late states were mainly distributed in acral melanoma and lymph node metastases samples, while the intermediate state was predominated in cutaneous melanoma (**Figure 4C**). The transition distributions were different among acral, cutaneous and lymph node metastasis melanoma (**Figure 4C**). As compared with cutaneous melanoma, the exhausted signature score of acral melanoma was significantly higher (See **Methods; Figure 4D**), while the cytotoxicity signature and resident scores were significantly lower (**Figure 4D**).

These six CD8 + T cell subgroups were categorized into 3 phases based on transcriptional changes along developmental trajectories (**Figure 4E**). The phase 1 was predominated by CD8-CCR7 and CD8-NR4A1 subgroups. Functional analysis showed that phase 1 was involved in positive regulation of lymphocyte activation, cellular response to heat, and cellular response to tumor necrosis factor. Phase 2 was characterized by the high expression of classical cytotoxic genes and low expression of T cell exhaustion markers. Phase 2 was involved in detoxification of copper ion (associated with *MT1E* and *MT2A*), antigen processing and presentation, and Wnt signaling pathway (**Figure 4E**). Phase 3 was characterized by high

levels of T cell exhaustion-related markers and associated with response to decreased oxygen levels (**Figure 4E)**. Among acral, cutaneous and lymph node metastasis melanoma, *GNLY* and *GZMA* appear to be up-regulated in Phase 2 but down-regulated in Phase 3 (**Figure 4F**). *GZMB* and *PRF1* were up-regulated from the beginning of the phase 2 towards the end of development, and were more prominent in acral melanoma (**Figure 4F**). In the phase 3, *PDCD1 (PD-1)* and *HAVCR2 (TIM-3)* were highly expressed in acral melanoma, while *CTLA4, TIGIT,* and *LAG3* were more prominent in cutaneous melanoma (**Figure 4G**). Compared with cutaneous melanoma, CD8+ T cells of acral melanoma were more in the initial state and exhausted state, lacking cytotoxicity. These also indicated that acral melanoma patients are more likely to develop resistance to immunotherapy. In addition, the exhausted CD8+ T cells of acral melanoma patients were characterized by high expression of *PDCD1 (PD-1)* and *HAVCR2 (TIM-3)*. Therefore, selective multi-target immunotherapy may benefit acral melanoma patients.

### Differences before and after treatment in an immune-resistant patient with acral melanoma

We compared the changes in the proportion of immune cells in the two acral melanoma samples (Acral3-pre and Acral3-post) before and after immunotherapy in one patient. It was found that the pre-treatment samples had more CD8+ T and Cycle T cells, while the post-treatment one was more prominent in CD4+ T and B cells (**Figure 5A**). We also identified the differentially expressed genes (DEGs) of CD8+ T cells between these two samples (**Figure 5B**). The pathways of immune functions were upregulated in pre-treatment such as antigen processing and presentation and NF-kappa B signaling, while those pathways were not enriched in post-treatment sample (**Figure 5C**). In addition, we compared the developmental trajectories of CD8+ T cells before and after the treatment. CD8+ T cells in the phase 2 of trajectory, cytotoxic CD8+T cells, were higher abundance before the anti-PD1 therapy (**Figure 5D** and **5E**), and genes (*GNLY*, *GZMB* and *PRF1*) related to cytotoxicity also showed high expression levels (**Figure 5F, Supplementary figure S1A-B**). The phenomenon indicated that the cytotoxicity of CD8+ T cells was reduced and the original immune-related functions were defuncted after receiving anti-PD1 therapy.

We also found that the genomic amplification of chromosome 4 was apparent in melanoma cells of the post-treatment sample but absent in those of pre-treatment sample (**Figure 5G**). Further analysis identified 44 genes in chromosome 4 was significantly amplified in the post-treatment sample as compared with the pre-treatment sample (See Methods, **Figure 5G**). The differential expression levels of these 44 genes from clinical trial (NCT01621490) dataset were higher in patients resistant to immunotherapy (PD, evaluated by Recist1.1) than those who are responsive[14] (CR and PR, **Figure 5H**). Meanwhile, 5 of these genes (*ANXA5*, *NAA15*, *ABCE1*, *ANAPC10* and *BBS7*) were significantly overexpressed in SD and PD patients compared to CR and PR patients (Kruskal-Wallis test, **Figure 5I**). These 44 genes were enriched in EGFR signaling and cell cycle phase transition (**Supplementary figure S1C**).

# Discussion

We provided a single-cell transcriptome landscape for acral melanoma in comparison with cutaneous melanoma. Our study provided a broad understanding of tumor microenvironment and cellular composition in acral melanoma. We unveiled 5 functional signatures from melanoma cells and linked them to the prognosis. Acral melanoma is different from cutaneous melanoma in that acral melanoma patients are mainly composed of Signatures 1 and 4, which are related to good prognosis. This finding was exemplified by the better overall survival of acral melanoma patients as compared with the cutaneous melanoma. Study from Lim and colleagues also reported that the overall survival of acral melanoma was better than that of non-acral melanoma patients[15] in Asian melanoma patient cohort.

In tumor immunity, Treg cells are involved in tumor development and progression by inhibiting antitumor immunity[16].Treg cells induced by the *PD-1* pathway may also assist in maintaining immune homeostasis, keeping the threshold for T-cell activation high enough to safeguard against autoimmunity[17]. We found that Treg cells were higher in acral melanoma than those in cutaneous melanoma. Higher abundance of Treg is associated with immunotherapeutic resistance. Thereby, we speculated that the response rate of acral melanoma is lower than cutaneous melanoma in the context of immunotherapy. Recent study showed that the ORR of acral melanoma (16%) was lower than the ORR of no-acral cutaneous melanoma (31%)[5,7]. An explanation to this observation is that infiltration of Treg prevent tumor cells from being killed by immune cells, and thus develop resistance to immune checkpoint inhibitors[18,19].

Acral melanoma had a high proportion of CD8 + T cells in the initial state and exhausted state. CD8 + T cells with cytotoxicity signature were relatively few in acral melanoma and quickly transformed into an exhausted state of high expression immunosuppressive marker genes. Our result revealed that *PDCD1 (PD-1)* and *HAVCR2TIM-3* were highly expressed in samples of acral melanoma, while *LAG3, TIGIT* and *CTLA4* displayed lower expression. Those indicated that combination of *PDCD1 (PD-1)* and *HAVCR2 (TIM-3)* blockades might benefit patients with acral melanoma. By contrast, patients with cutaneous melanoma were characterized by exhausted CD8 + T cells that expressed high level of *LAG3* and *CTLA4*. This implied that the combination of *LAG3* and *CTLA4* inhibitors might be more appropriate for cutaneous melanoma patients.

In the comparative analysis of samples before and after immunotherapy, it was showed that the patient's immune environment had undergone major changes. The post-treatment immune environment had more CD4 + T and B cells,while less CD8 + T and Cycle T cells comparing to the pre-treatment sample. The CD8 + T cells of the samples post-treatment had lost their original immune function, and the ratio of CD8 + T cells with cytotoxicity was reduced. These are probably the reasons why the anti-PD1 treatment of this acral melanoma patient was not effective.

Interestingly, we found that 44 genes from amplification of chromosome 4 in two samples that were resistant to immunotherapy. These 44 genes were enriched in *EGFR* and cell cycle pathway. A previous study showed that *EGFR* can up-regulate the expression of *PD-L1*, and causing immunosuppression. This means that immunotherapy combined with *EGFR* pathway related gene (*TRIM2*, *GAB1*, *SPRY1*) inhibitors may improve the effectiveness of immunotherapy[20]. In addition, we verified that these 44 genes exhibited

higher expression in the SD and PD group in comparison with CR + PR group. More specifically, we observed that 5 of them were significantly upregulated in SD and PD groups.

In conclusion, this study enables better understanding of the tumor ecosystem heterogeneity between acral and cutaneous melanoma, in terms of immune and tumor phenotypes. Our results can be a valuable resource, facilitating a deeper understanding of the mechanisms associated with acral melanoma and assisting in developing more effective therapeutic targets and biomarkers for immunotherapies in acral melanoma patients.

# Methods

### Sample collection

The tissue samples were obtained with patient informed consent and approval of the Tianjin Medical University Cancer Institute and Hospital. Fresh tumor samples were surgically removed from patients and immersed in a complete medium containing 90% Dulbecco's modified eagle medium (DMEM; Cat# 11054001, GIBCO) and 10% fetal bovine serum (FBS; Cat# 16140071, GIBCO), and transported to the lab in a refrigerated container. Suitable small tissue blocks were cut into pieces (diameter 1-3 mm). The pieces were transferred to the gentle MACS C Tubes (Cat# 130-096-334, Miltenyi Biotec), with 5 mL of digestive enzyme included in Tumor Dissociation Kit (Cat# 130-095-929, Miltenyi Biotec). Then the tissues were made into single-cell suspension using the gentle MACS Dissociator (Cat# 130-093-235, Miltenyi Biotec) following these steps: milled; incubated at 37℃ for 30 min on a shaker; milled; incubated at 37℃ for 30 min; milled; filtered through a 70 mm filter, plus 2% FBS. Finally, the single-cell suspension was centrifugated at 400 g for 7 mins, resuspended in CELLSAVING (Cat# C40050, NCM biotech), cryopreserved in Cryotubes (Cat# 430488, Corning) and then stored at -80℃.

### Single cell RNA sequencing

Cell suspensions were barcoded through the 10x Chromium Single Cell platform using the MGIEasy Universal Library Conversion kit (App-A) (Part Number:1000004155) before sequencing can be performed on the MGISEQ-2000 instrument. For each library, 10 ng was amplified using 10 cycles of polymerase chain reaction (PCR) to incorporate a 5' phosphorylation on the forward strand only. Purified PCR product was then denatured and mixed with a 'splint' oligonucleotide that is homologous to the P5 and P7 adapter regions of the library to generate a circle. A ligase reaction was then performed to create a complete ssDNA circle of the forward strand then an exonuclease digest was performed to remove single stranded non-circularized DNA molecules. Circular ssDNA molecules then underwent Rolling Circle Amplification (RCA) to generate 300–500 faithful copies of the libraries which then fold upon themselves to become DNA Nanoballs (DNB). Each DNB library was then flowed across a 1500 M feature patterned array flow cell ready for sequencing using the MGISEQ-2000RS High-Throughput Sequencing Set (App-A) (PE100) (Part Number: 1000005662). The custom cycle mode on the instrument was run to allow 28 bp

(Read 1) and 100 bp (Read2) cycles without an index barcode read due to only one sample being run per flow cell, and FASTQ files were generated locally on the instrument. Sequencing was performed in BGI Shenzhen, MGIR&D facility

## Single-cell sequencing analysis

Raw base call (BCL) files were analyzed using CellRanger (v2.1.1). The “mkfastq” command was used to generate FASTQ files and the “count” command was used to generate raw gene-barcode matrices aligned to the 10X Genomics GRCh38 Ensembl build 84 genome (v1.2.0). The data from all 7 samples were combined in R (v3.6.2) using the Read10X function from the Seurat package (v3.1.5), and an aggregate gene expression matrix and Seurat object (63,394 samples and 35124 genes) were generated. The gene expression matrix was normalized by log2 transformation and scaled each gene by subtracting its mean and dividing with standard deviation. The gene expression signatures of single cells were captured by deep neural network. In this study, Momentum Contrast algorithm[21,22] was used to learn similar representation of single cell expression by narrowing the gap between the augmented and corresponding original gene expression profiles, which consisted of a deep neural network of 63 layers with dense connection as feature encoder and multi-layer perceptron (MLP) as project head to map features learned by the encoder network to space where contrastive learning is applied. Data augmentation was used to increase data diversity and mimic data variation, and the operations included random shuffling or zeroing out 20% of gene expression values. Stochastic gradient descent algorithm[23] was used to train the model in parallel on two graphic processing units for 299 epochs with an initial learning rate of 0.24, weight decay of 0.0001 and batch size of 256. The learning rate was decayed by 0.1 at epoch 150 and 250. The model was developed with PyTorch package (v 2.3.1). The K-nearest neighbor graph was built on gene expression signatures of single-cells using Scanpy[24] (v2.1). The gene expression signatures of single-cell were embedded into two dimensions by t-distributed stochastic neighbor embedding[25] (*t*-SNE). The neighbor graph was used to find clusters by Leiden algorithm[26]. and a n-neighbors parameter set to “k = 5”. The cluster-specific marker genes were identified by MAST algorithm[27] using Seurat “FindAllMarkers” function. The resulting single-cell clusters were visualized in *t*-SNE representations and annotated to biological cell types by canonical marker genes (**Figure 1C**).

## Composition of acral melanoma

The acral melanoma tumor cell subgroups were clustered based the biological function, and the shared genes of these clusters were identified as the marker genes of melanoma tumor function modules. Single-sample Gene Set Enrichment Analysis (ssGSEA)[28] was used to calculate separate enrichment score of function module for each melanoma sample in TCGA[12]. The melanoma cohort was clustered subgroup using Non-negative Matrix Factorization (NMF) algorithm[29].

## Cell developmental trajectory

The cell lineage trajectory of CD8+ T was inferred by using Monocle2[30]. We excluded CD8-HOPX and CD8-EOMES cells according to their TCR identity due to their distinct TCRs and development processes relative to other CD8+ cells. We first used the “relative2abs” function in Monocle2 to convert TPM into normalized mRNA counts and created an object with parameter “expressionFamily = negbinomial.size” following the Monocle2 tutorial. We used the “differentialGeneTest” function to derive DEG from each cluster and genes with a q-value < 1e-5 were used to order the cells in pseudotime analysis. After the cell trajectories were constructed, differentially expressed genes along the pseudotime were detected using the “differentialGeneTest” function.

## Pathway analysis and functional annotation

We used Gene Ontology enrichment analysis and Single-sample Gene Set Enrichment Analysis (ssGSEA) for functional analysis. Gene signatures scores of samples were evaluated using R package gsva. GO and KEGG analyses were performed by applying the “clusterProfiler” package.

## Definition of cell scores and signatures

We used the average expression (measured by log2 (CPM + 1) of 5 resident markers (*RUNX3*, *NR4A1*, *CD69*, *CXCR6*, and *NR4A3*), 7 cytotoxicity associated genes (*PRF1*, *IFNG*, *GNLY*, *NKG7*, *GZMB*, *GZMA*, *CST7*, and *TNFSF10*), 5 exhausted markers (*CTLA4*, *HAVCR2 /TIM-3*, *LAG3*, *PDCD1/PD-1*, and *TIGIT*) and 6 costimulatory molecular genes (*ICOS*, *CD226*, *TNFRSF14*, *TNFRSF25*, *TNFRSF9*, and *CD28*) to define the resident, cytotoxic, exhausted, and costimulatory score for CD8+ T cells. We used non-negative matrix factorization algorithm implemented in R package NMF (v 0.23.0) to extract the characteristics of samples based on the identified gene module scores. The features of malignant cells were defined with the mean log2 (CPM + 1) normalized expression of 5 modules signature genes (**Table S2**).

## Survival analysis

Kaplan-Meier survival was used to analyze the prognosis of acral melanoma and cutaneous melanoma by R package survival (v 3.1.12). We used the log-rank test to calculate differences of survival curves.

## Identification of differentially expressed genes

We considered CD8+ T cells from different states of Acral3 sample to identify the DEGs between before and after the PD-1 treatment. The “limma” package was used to identify DEGs with a P value <0.05 and logFC >0.5.

## CNV analysis of single-cell

The large-scale chromosomal copy number variations of melanoma tumor cells were identified using inferCNV R routine (version 1.5.1). The chromosomal region in genetic profiles was inferred based on the average expression of single-cells. A random sample of 1000 tumor cells were taken from each sample, and stromal cells (1,938 endothelial cells and 1,624 fibrocytes) were taken into control group. Other parameters were set as default. The comparisons of patients with different immunotherapy RECIST outcome were performed using the gene expression variation between pretherapy and post-treatment.

### Statistics Analysis

Cell distribution comparisons between acral melanoma and cutaneous melanoma were performed using Student's *t*-test. All statistical analyses and presentation were performed using R. Statistical tests used in figures were shown in figure legends and statistical significance was set at $p < 0.05$. Two-sided test was used if not specified.

# Declarations

### Conflict of interest

The authors declare that they have no competing interests.


### Acknowledgments

We thank professor Wei Zhang of Wake Forest Baptist Comprehensive Cancer Center for his valuable suggestions to the design and analysis of this article.


# References


1. Basurto-Lozada, P.*, et al.* Acral lentiginous melanoma: Basic facts, biological characteristics and research perspectives of an understudied disease. *Pigment cell & melanoma research* **34**, 59-71 (2021).

2. Yeh, I.*, et al.* Targeted Genomic Profiling of Acral Melanoma. *Journal of the National Cancer Institute* **111**, 1068-1077 (2019).

3. Furney, S.J.*, et al.* The mutational burden of acral melanoma revealed by whole-genome sequencing and comparative analysis. *Pigment cell & melanoma research* **27**, 835-838 (2014).

4. Hodi, F.S.*, et al.* Imatinib for melanomas harboring mutationally activated or amplified KIT arising on mucosal, acral, and chronically sun-damaged skin. *Journal of clinical oncology : official journal of the American Society of Clinical Oncology* **31**, 3182-3190 (2013).

5. Tang, B.*, et al.* Safety, Efficacy, and Biomarker Analysis of Toripalimab in Previously Treated Advanced Melanoma: Results of the POLARIS-01 Multicenter Phase II Trial. *Clinical cancer research : an*

*official journal of the American Association for Cancer Research* **26**, 4250-4259 (2020).

6. Hamid, O.*, et al.* Safety and Tumor Responses with Lambrolizumab (Anti–PD-1) in Melanoma. **369**, 134-144 (2013).

7. Nakamura, Y.*, et al.* Anti-PD1 checkpoint inhibitor therapy in acral melanoma: a multicenter study of 193 Japanese patients. *Annals of oncology : official journal of the European Society for Medical Oncology* **31**, 1198-1206 (2020).

8. Greaves, W.O.*, et al.* Frequency and spectrum of BRAF mutations in a retrospective, single-institution study of 1112 cases of melanoma. *The Journal of molecular diagnostics : JMD* **15**, 220-226 (2013).

9. Tirosh, I.*, et al.* Dissecting the multicellular ecosystem of metastatic melanoma by single-cell RNA-seq. *Science (New York, N.Y.)* **352**, 189-196 (2016).

10. de Andrade, L.F.*, et al.* Discovery of specialized NK cell populations infiltrating human melanoma metastases. *JCI insight* **4**(2019).

11. Sade-Feldman, M.*, et al.* Defining T Cell States Associated with Response to Checkpoint Immunotherapy in Melanoma. *Cell* **175**, 998-1013.e1020 (2018).

12. Zhang, T., Dutton-Regester, K., Brown, K.M. & Hayward, N.K. The genomic landscape of cutaneous melanoma. *Pigment cell & melanoma research* **29**, 266-283 (2016).

13. Trapnell, C.*, et al.* The dynamics and regulators of cell fate decisions are revealed by pseudotemporal ordering of single cells. *Nature biotechnology* **32**, 381-386 (2014).

14. Riaz, N.*, et al.* Tumor and Microenvironment Evolution during Immunotherapy with Nivolumab. *Cell* **171**, 934-949.e916 (2017).

15. Lim, Y., Lee, J. & Lee, D.Y. Is the survival rate for acral melanoma actually worse than other cutaneous melanomas? *The Journal of dermatology* **47**, 251-256 (2020).

16. Ohue, Y. & Nishikawa, H. Regulatory T (Treg) cells in cancer: Can Treg cells be a new therapeutic target? *Cancer science* **110**, 2080-2089 (2019).

17. Francisco, L.M., Sage, P.T. & Sharpe, A.H. The PD-1 pathway in tolerance and autoimmunity. *Immunological reviews* **236**, 219-242 (2010).

18. Tanaka, A. & Sakaguchi, S. Targeting Treg cells in cancer immunotherapy. *European journal of immunology* **49**, 1140-1146 (2019).

19. Saleh, R. & Elkord, E. Treg-mediated acquired resistance to immune checkpoint inhibitors. *Cancer letters* **457**, 168-179 (2019).

20. Li, T.*, et al.* IGFBP2 regulates PD-L1 expression by activating the EGFR-STAT3 signaling pathway in malignant melanoma. *Cancer letters* **477**, 19-30 (2020).

21. Chen, X., Fan, H., Girshick, R. & He, K. Improved Baselines with Momentum Contrastive Learning (2020).

22. He, K., Fan, H., Wu, Y., Xie, S. & Girshick, R. Momentum Contrast for Unsupervised Visual Representation Learning. (2019).

23. Bottou, L. Stochastic gradient descent tricks. in *Neural networks: Tricks of the trade* 421-436 (Springer, 2012).

24. Wolf, F.A., Angerer, P. & Theis, F.J. SCANPY: large-scale single-cell gene expression data analysis. *Genome Biol* **19**, 15 (2018).

25. Linderman, G.C., Rachh, M., Hoskins, J.G., Steinerberger, S. & Kluger, Y. Fast interpolation-based t-SNE for improved visualization of single-cell RNA-seq data. *Nat Methods* **16**, 243-245 (2019).

26. Traag, V.A., Waltman, L. & van Eck, N.J. From Louvain to Leiden: guaranteeing well-connected communities. *Sci Rep* **9**, 5233 (2019).

27. Finak, G.*, et al.* MAST: a flexible statistical framework for assessing transcriptional changes and characterizing heterogeneity in single-cell RNA sequencing data. *Genome Biol* **16**, 278 (2015).

28. Subramanian, A.*, et al.* Gene set enrichment analysis: a knowledge-based approach for interpreting genome-wide expression profiles. *Proceedings of the National Academy of Sciences of the United States of America* **102**, 15545-15550 (2005).

29. Lee, D.D. & Seung, H.S. Learning the parts of objects by non-negative matrix factorization. *Nature* **401**, 788-791 (1999).

30. Qiu, X.*, et al.* Reversed graph embedding resolves complex single-cell trajectories. *Nature methods* **14**, 979-982 (2017).

# Figures

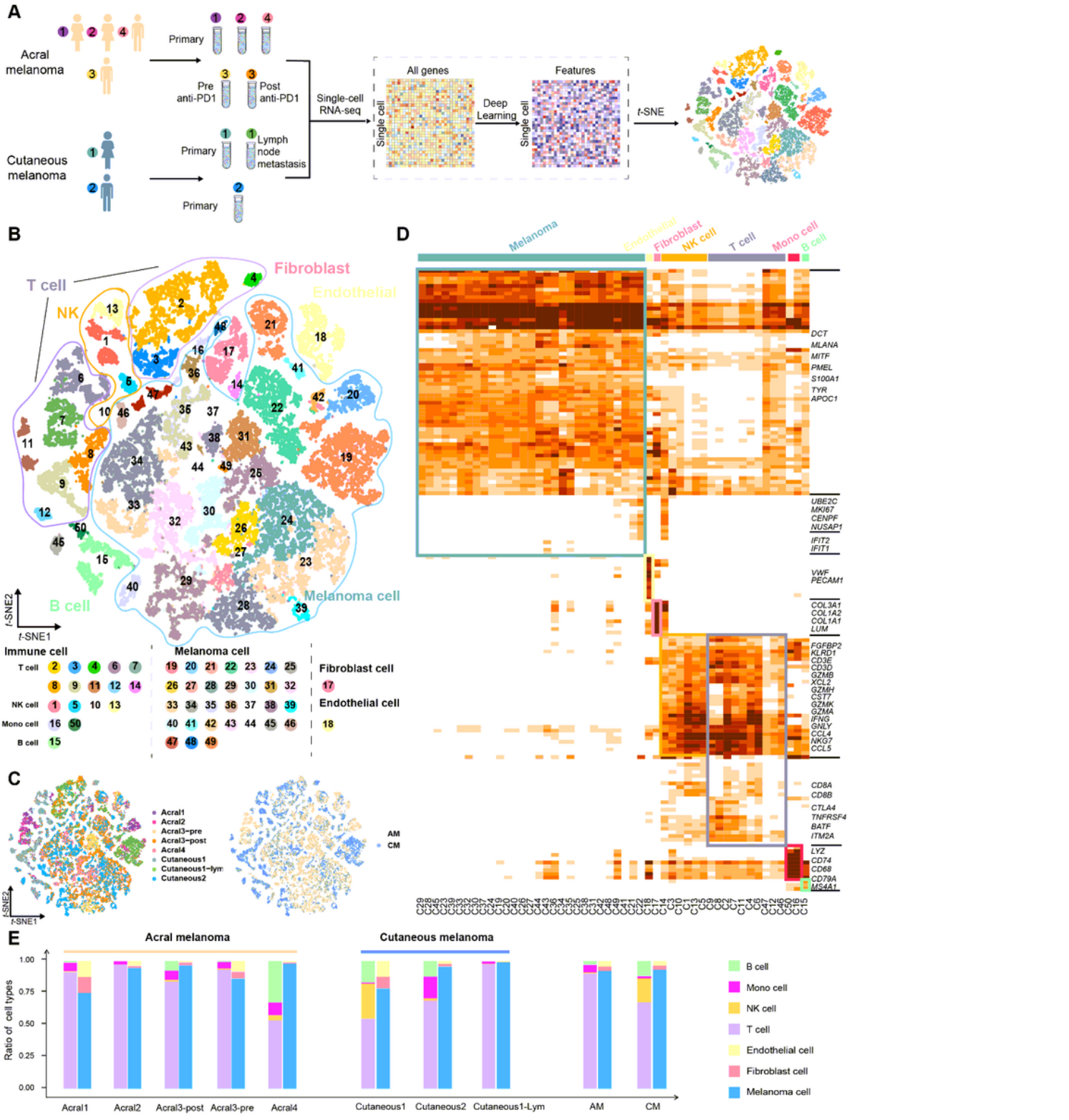


## Figure 1

ScRNA-seq profiling of the acral and cutaneous melanoma environments (A) Schematic representation of the experimental strategy. (B) T-distributed stochastic neighbor embedding (t-SNE) plot, showing the annotation and color codes for cell types in the melanoma ecosystem. (C) The t-SNE plot, showing cell origins by color, patient origin (left panel), and Acral melanoma or Cutaneous melanoma origin (right panel). (D) Heatmap showing the expression of marker genes in the 50 cell clusters. The top bars label

the clusters corresponding to specific cell types. (E) Histogram indicating the proportion of cells in tumor tissue of each analyzed patient. Non-immune cells and immune cells are shown in separate histograms.

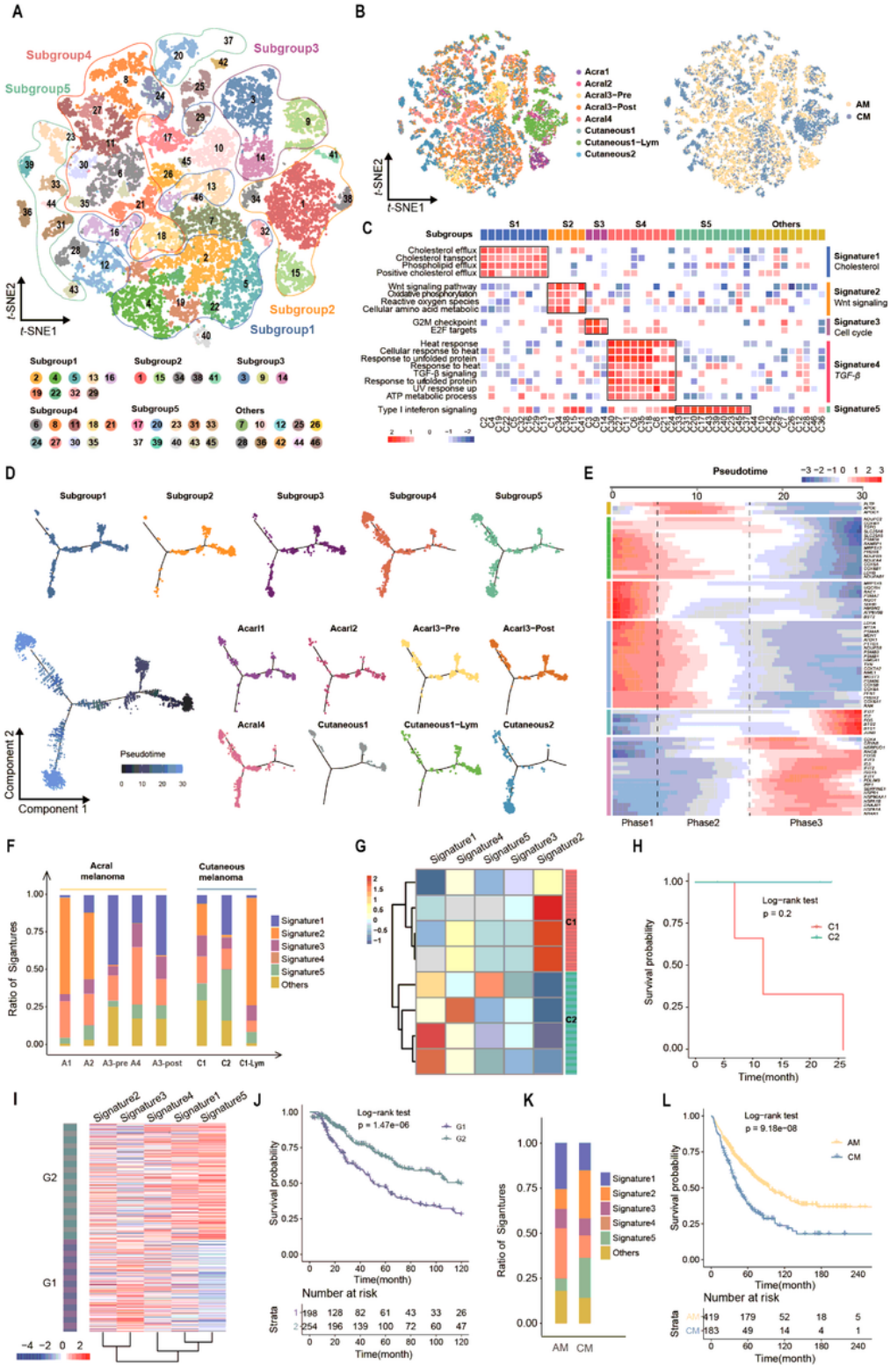


## Figure 2

5 subgroups of melanoma cells (A) t-SNE plot showing the clusters and subgroups of melanoma cells. 5 subgroups are circled with corresponding colors. (B) t-SNE plot showing the cell origins by color, according to the samples (left panel) or subtypes (Acral melanoma/Cutaneous melanoma, right panel).

(C) Heatmap showing the expression score by ssGESA in the 46 clusters (5 Signatures), including biological functions and names of related signal pathways. (D) Pseudotime-ordered analysis of melanoma cells from Acral melanoma and Cutaneous melanoma samples. Melanoma subgroups and samples are labeled by colors. (E) Heatmap showing the dynamic changes in gene expression along the pseudotime. (F) Histogram indicating the proportion of signatures in melanoma of each analyzed samples. (G) Heatmap showing the signature ratio of 8 single-cell samples and clustering into C1 and C2. (H) Kaplan-Meier analysis showing the overall survival rate of 6 patients, characterized by C1 (red) and C2 (green). (I) Heatmap showing the expression score of 452 TCGA-SKCM patient's bulk-RNA data by ssGESA in the 5 signatures, including 2 clusters of NMF. (J) Kaplan-Meier analysis showing the overall survival rate of 452 TCGA-SKCM patients, characterized by C1 (purple) and C2 (dark green). The numbers of patients and the risk classification are indicated in the figure. Significance was calculated using the log-rank test. (K) Histogram indicating the proportion of signatures in 4 acral samples (Acral1, Acral2, Acral3-pre, Acral4) and 3 cutaneous samples (Cutaneous1, Cutaneous2, Cutaneous1-lym). (L) Kaplan-Meier analysis showing the overall survival rate of 602 inner patients, characterized by Acral melanoma (yellow) and Cutaneous melanoma (blue). The numbers of patients and the risk classification are indicated in the figure. Significance was calculated using the log-rank test

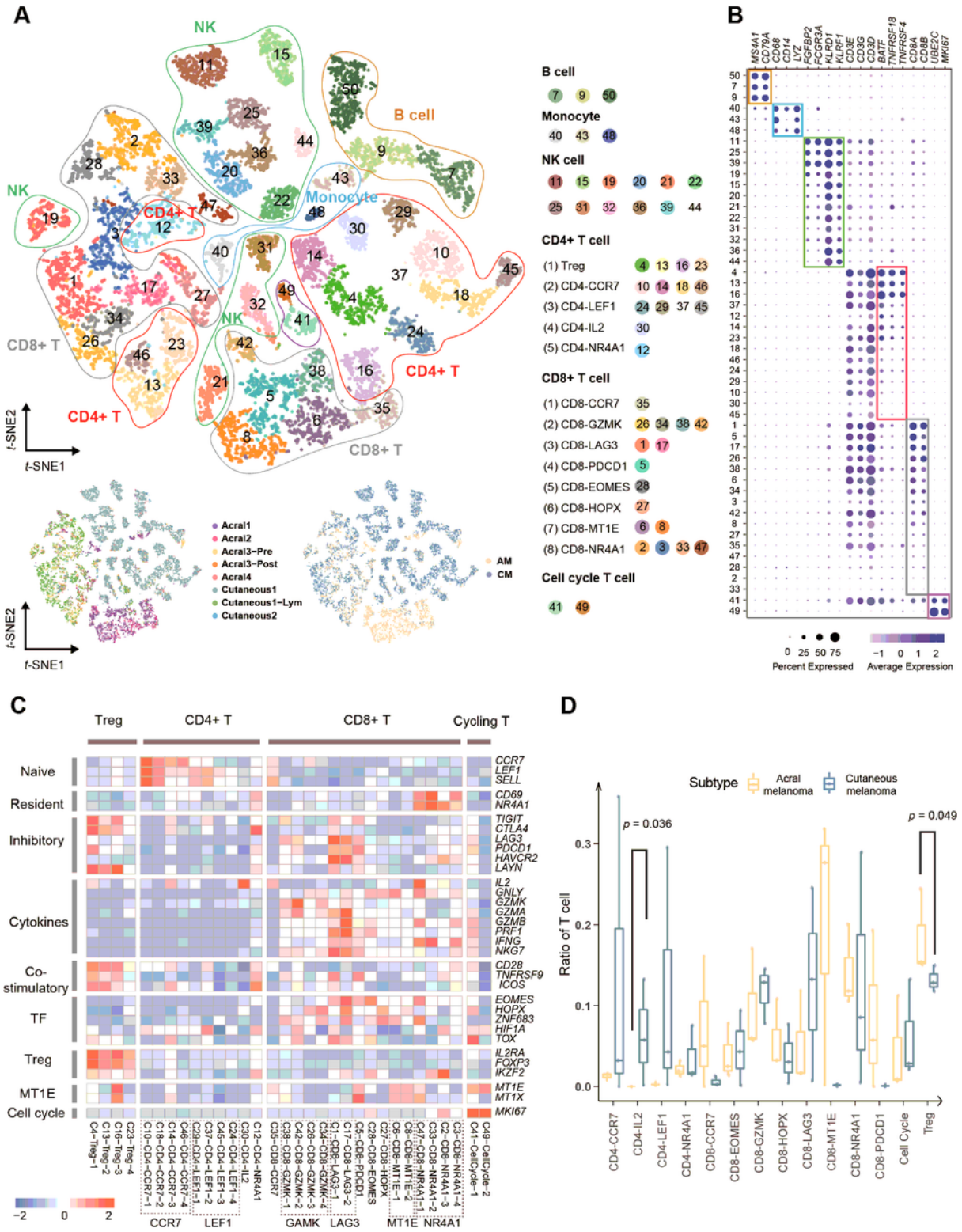


## Figure 3

Immune cell components in acral and cutaneous melanoma. (A) t-SNE plot showing the clusters of immune cells and cell origins by color, according to immune cell types (upper panel), samples (lower left panel) and subtypes (Acral melanoma/Cutaneous melanoma, lower right panel). (B) Dot plot showing percent expression and average expression of 50 immune cell clusters, including 6 main types of immune cells. (C) Heatmap indicating the expression of selected gene sets in T subtypes, including naive, resident,

inhibitory, cytokines, co-stimulatory, transcriptional factors (TF), Treg , MT1E, cell cycle and cell type. (D) Boxplots illustrating the fraction of T subtypes in Acral melanoma (yellow; Acral1, Acral2, Acral3-pre, Acral4 ) and Cutaneous melanoma (blue; Cutaneous1, Cutaneous2, Cutaneous1-lym), respectively.

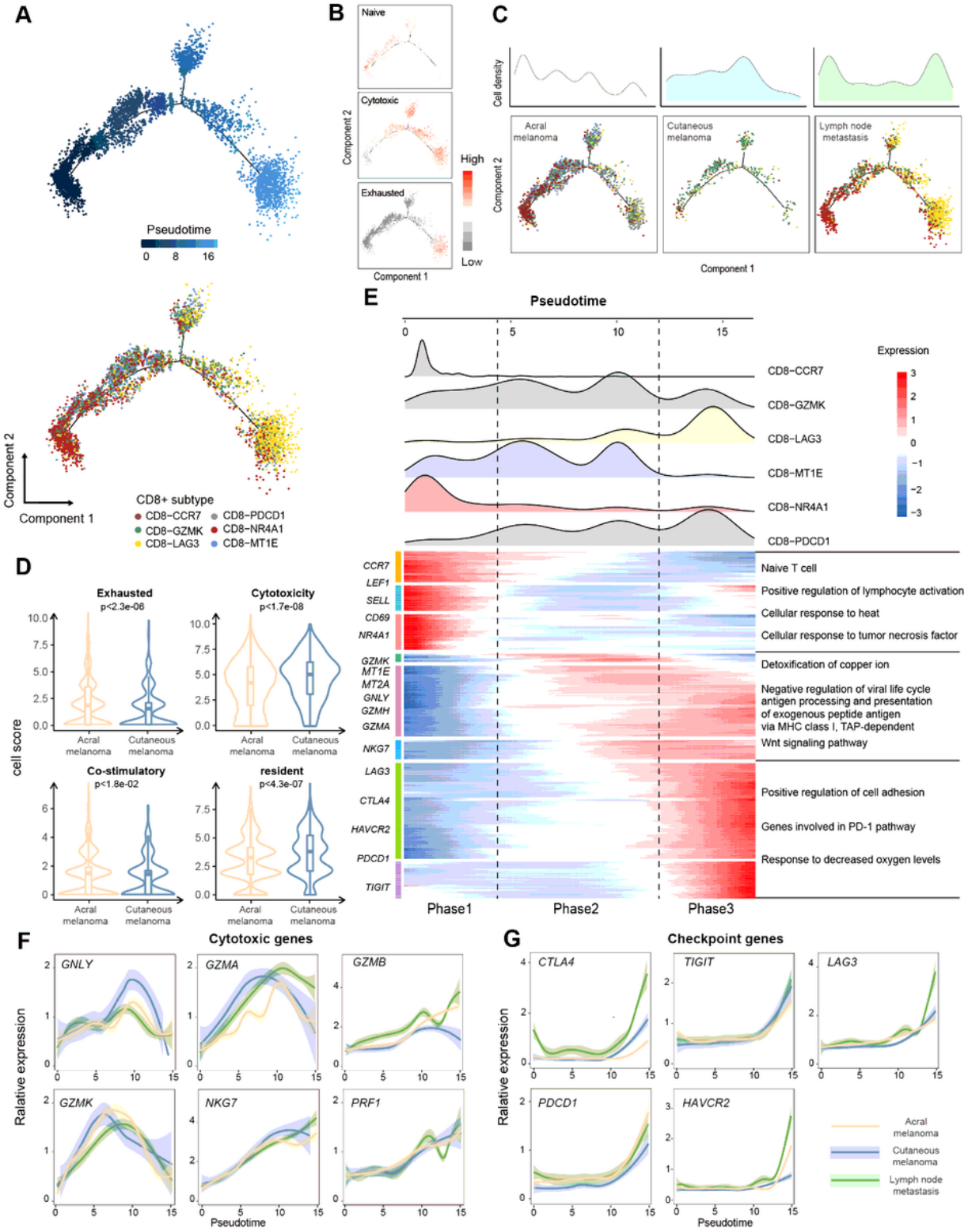


## Figure 4

Analysis of CD8 + T cell transition states in Acral melanoma and Cutaneous melanoma samples (A) Pseudotime-ordered analysis of CD8 + T cells from Acral melanoma and Cutaneous melanoma samples.

T cell subtypes are labeled by colors. (B) 2D pseudotime plot showing the dynamics of naïve (upper panel), cytotoxic (middle panel) or exhausted signals (lower panel) in CD8 + T cells, from Acral melanoma and Cutaneous melanoma samples. (C) 2D graph of the pseudotime-ordered CD8+T cells, from Acral melanoma (left panel), Cutaneous melanoma (middle panel) and Lym (right panel) samples. The cell density distribution, by state, is shown at the top of the figure. (D) Violin plot showing the expression of co-stimulatory, cytotoxic, resident, and inhibitory signature genes in CD8 + T cells in Acral melanoma (yellow; Acral1, Acral2, Acral3-pre, Acral4) and Cutaneous melanoma (blue; Cutaneous1, Cutaneous2) samples. Significance was determined by Student's t test. (E) Heatmap showing the dynamic changes in gene expression along the pseudotime (lower panel). The distribution of CD8 subtypes during the transition (divided into 3 phases), along with the pseudo-time. Subtypes are labeled by colors (upper panel). (F and G) Two-dimensional plots showing the dynamic expression Cytokines genes(F) and checkpoint genes (G) during the T cell transitions along the pseudo-time.

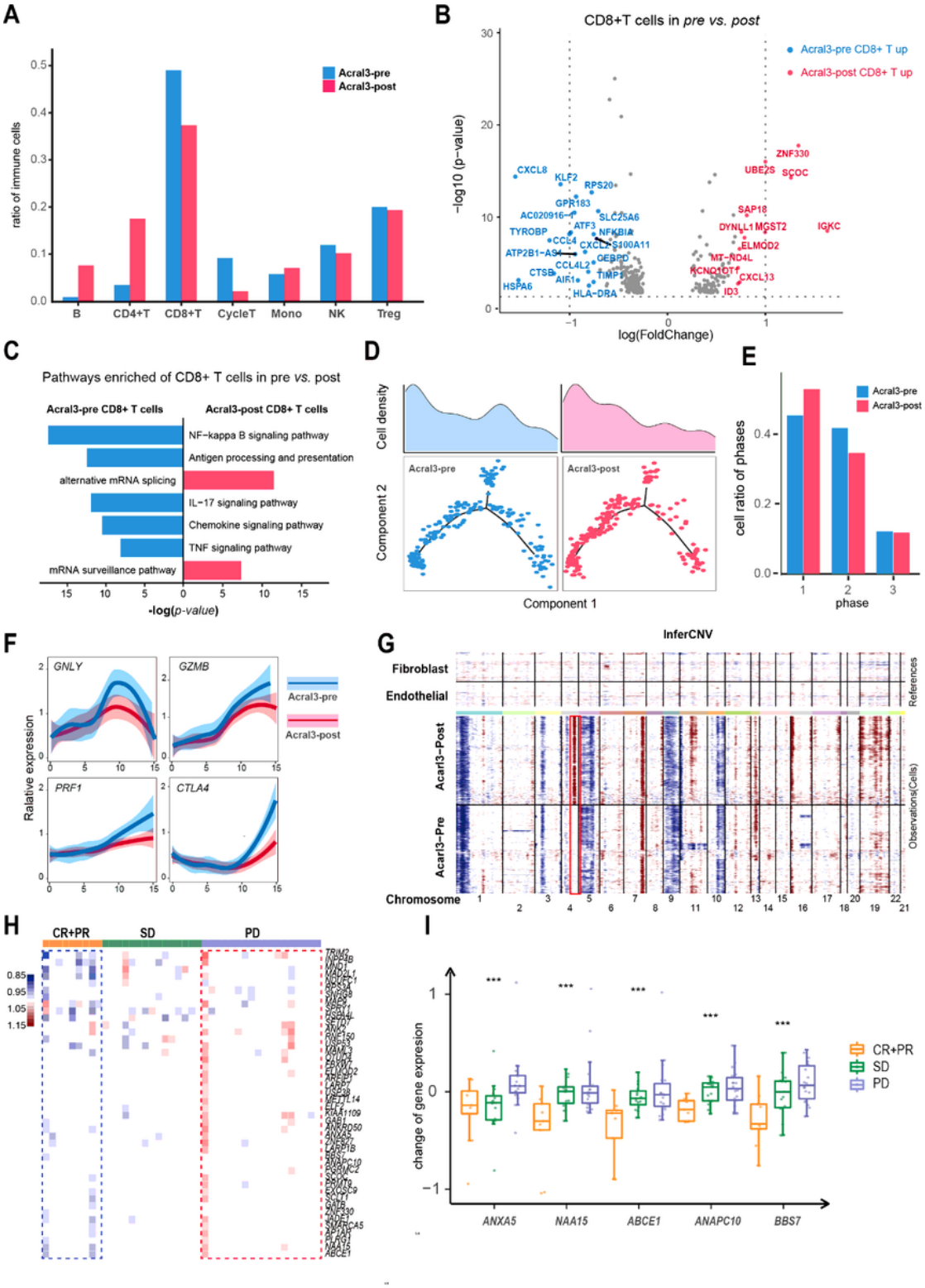


## Figure 5

Differences before and after treatment in an immune-resistant patient with acral melanoma (A) Histogram showing the difference in ratio of immune cells subtypes between the pre-treatment and post-treatment samples (B) Volcano plot shows differentially expressed genes between Acral3-pre CD8+ T cells (blue dots) and Acral3-post CD8 + T cells (red dots). The names of the most significant genes are indicated in the plots (C) Two-sided bar graph showing the enriched activated pathways between CD8 + T

cells of the Acral3-pre and Acral3-post (D) 2D graph of the pseudotime-ordered CD8+T cells, from Acral3-pre (left panel) and Acral3-post (right panel) samples. The cell density distribution, by state, is shown at the top of the figure. (E) Histogram showing the difference in the phase of CD8+ T cells between the pre-treatment and post-treatment samples (F) Dimensional plots showing the dynamic expression of cytokines genes and checkpoint genes during the T cell transitions along the pseudo-time. (G) Representative CNV heatmaps with hierarchical clustering from inferCNV analysis from a pair of samples (Acral-3 pre and Acral3-post) before and after receiving immunotherapy. (H) Heatmap showing the changes of 44 gene expression in matching samples received anti-PD1 therapy. (I) Boxplot shows the genes with significant differences in the CR+PR, SD, and PD groups.

## Supplementary Files

This is a list of supplementary files associated with this preprint. Click to download.

- Supplement.docx